AIAA JOURNAL
Vol. 31, No. 10, October 1993

Flutter Analysis of Stiffened Laminated Composite Plates and Shells in Supersonic Flow

Chung-Li Liao* and Yee-Win Sun†
National Taiwan Institute of Technology, Taipei, 107 Taiwan, Republic of China

This paper investigates the flutter instability of stiffened and nonstiffened laminated composite plates and shells subjected to aerodynamic forces in the supersonic flow. The equation of motion of the present problem is formulated using Hamilton's principle. Then, using the finite element method along with three-dimensional degenerated shell elements and three-dimensional degenerated curved beam elements, the equation of motion is discretized. The characteristic equation to study the flutter instability of the present problem is obtained from the previous finite element equation of motion. Finally, natural frequency, critical dynamic pressure, and corresponding flutter mode shape are found by solving the characteristic equation. The effects of various parameters, such as skew angle, lamination scheme, subtended angle, and stiffening scheme on the flutter instability of stiffened and nonstiffened plates and shells in the supersonic flow are demonstrated through the numerical examples.

I. Introduction

FOR the aircraft structure subjected to aerodynamic loading, the interactions between elastic deformation of structure and aerodynamic forces can make the structure unstable, i.e., flutter or divergence may develop. As a consequence, the onset of instability may induce disastrous structural failure or undesirable limit cycle oscillations. Since the aeroelastic stability is an important problem, many flutter analyses of aircraft structure in supersonic and subsonic flow have already been done. Both linear and nonlinear (due to large deflections) flutter analyses were considered in the past. In 1970 Dowell[1] gave a comprehensive review on both linear and nonlinear panel flutter.

Applications of the finite element method in the aeroelastic analysis have been performed by many investigators (for example, Refs. 2–16). Some of them[2–13] studied the linear flutter problems and indicated that there is a critical (or flutter) dynamic pressure above which the motion of the external skin (or panel) of the aircraft becomes unstable and grows exponentially with time. Since the linear flutter analysis does not include the structural geometric nonlinearity (i.e., large deflections), it can determine only the flutter boundary and can give no information about the flutter oscillation itself. Nonlinear flutter analysis[14–16] found that the geometrically nonlinear effects restrain the panel motion to bounded limit cycle oscillations with increasing amplitude as the dynamic pressure increases.

Composite material has been increasingly employed in aircraft structures (e.g., wing skin) due to its light weight and high strength/stiffness-to-weight ratio. However, studies on aeroelastic behavior of laminated composite structures are not many.[11–13,17] Also, most of the previous studies on panel flutter analysis are concerned with plates and cylindrical shells. The aeroelastic analysis of stiffened plates or shells is seldom seen in the literature. Because in aircraft structures (such as fuselage, wings, engine housings, etc.) panels with stiffeners are very popular for the purpose of saving weight, their aeroelastic behaviors deserve further investigation. The present work attempts to study the flutter phenomena of stiffened isotropic and laminated composite plates and shells subjected to supersonic aerodynamic forces. Two-dimensional quasi-steady aerodynamic theory is adopted for the evaluation of aerodynamic forces. The mathematical model for this problem is formulated using Hamilton's principle and then discretized by the finite element method. Three-dimensional degenerated shell elements and three-dimensional degenerated curved beam elements are employed to model plates/shells and stiffeners, respectively. The compatibility between the shell element and the stiffener element is retained. Only the linear analysis is considered here. By obtaining the characteristic curves of natural frequencies vs dynamic pressure, the effects of various parameters, such as skew angle, lamination scheme, subtended angle, and number and position of stiffener, on the flutter instability of stiffened plates and shells in supersonic flow are examined numerically.

II. Governing Equations

Linear theory, i.e., assuming small deformations of the stiffened plate or shell, is adopted here because we intend to understand the effects of dynamic pressure on the natural vibration frequencies of stiffened plates or shells and to find the magnitudes of dynamic pressure that make the structure unstable. Large deformation theory should be used if the postflutter behavior is to be studied. For a panel, stiffened or nonstiffened, subjected to aerodynamic forces, the mathematical model to govern its motion can be obtained using Hamilton's principle, which states that

$$\int_{t_1}^{t_2} (\delta T - \delta U)\, \mathrm{d}t + \int_{t_1}^{t_2} \delta W\, \mathrm{d}t = 0$$

$$[\delta u_i(t_1) = 0, \quad \delta u_i(t_2) = 0] \tag{1}$$

where δT and δU are the first variations of kinetic energy and strain energy of the system, respectively, δW is the virtual work done by the aerodynamic forces (a nonconservative force field), $\delta u_i(t_i)$ is the virtual displacements at time t_i, and t_1 and t_2 are the initial and final times of the motion, respectively. The variables δU and δT are expressed as

$$\delta U = \int_V \sigma_{ij} \delta \epsilon_{ij}\, \mathrm{d}V \tag{2}$$

$$\delta T = \int_V \rho \ddot{u}_i \delta \epsilon \dot{u}_i\, \mathrm{d}V \tag{3}$$

Received Sept. 23, 1992; revision received Jan. 21, 1993; accepted for publication Jan. 21, 1993.

*Associate Professor, Department of Mechanical Engineering.
†Graduate Student, Department of Mechanical Engineering.

where σ_{ij} and ϵ_{ij} are the rectangular Cartesian components of the Cauchy stress tensor and the infinitesimal strain tensor, respectively, $\dot{u}_i$ is the rectangular Cartesian component of the velocity vector, and the integrations are performed over the volume of panel V. If we consider a skew plate, an oblique Cartesian coordinate system should be used, and σ_{ij} are the contravariant components of the Cauchy stress tensor, and ϵ_{ij} are the covariant components of the infinitesimal strain tensor.[18] Since we adopted the two-dimensional quasisteady aerodynamic theory[19] to evaluate the aerodynamic pressure, δW in Eq. (1) can be written as

$$\delta W = \int_A p(x_1, x_2, t)\, \delta u_3\, dA \tag{4}$$

where $p(x_1, x_2, t) = -[\lambda(\partial u_3/\partial x_1) + g(\partial u_3/\partial t)]$ = aerodynamic pressure.

$$\lambda = \frac{2q}{(M^2-1)^{0.5}} = \frac{\rho_a U_a^2}{(M^2-1)^{0.5}}$$

$$g = \frac{\lambda}{U_a}\frac{M^2-2}{M^2-1} = \frac{\rho_a U_a (M^2-2)}{(M^2-1)^{1.5}}$$

$$q = \tfrac{1}{2}\rho_a U_a^2$$

where ρ_a is the air mass density, U_a the freestream airflow velocity, q the dynamic pressure, M the Mach number, x_1 the direction of airflow, and u_3 the panel displacement normal to the panel midsurface.

The integration in Eq. (4) is performed over the midsurface of the plate/shell A. Introduce a parameter $\mu = \rho_a a/(\rho h)$, which is the mass density ratio of air to the plate/shell, where ρ is the mass density of the plate/shell, a is the side length of the plate/shell, and h is the thickness of the plate/shell. Hence we can express g as a function of λ and μ (Ref. 15), i.e.,

$$g^2 = \frac{\lambda^2}{U_a^2}\left(\frac{M^2-2}{M^2-1}\right)^2 = \frac{\rho_a^2 U_a^2}{M^2-1}\left(\frac{M^2-2}{M^2-1}\right)^2$$

$$= \frac{\rho_a U_a^2}{(M^2-1)^{0.5}}\frac{\rho_a}{(M^2-1)^{0.5}}\left(\frac{M^2-2}{M^2-1}\right)^2$$

$$= \lambda\frac{\rho h \mu}{a}\frac{1}{(M^2-1)^{0.5}}\left(\frac{M^2-2}{M^2-1}\right)^2$$

When $M \gg 1$,

$$\frac{\mu}{(M^2-1)^{0.5}}\left(\frac{M^2-2}{M^2-1}\right)^2 \cong \frac{\mu}{M}$$

So that g can be written as

$$g = \left(\frac{\mu}{M}\right)^{0.5}\left(\frac{\rho h \lambda}{a}\right)^{0.5} \tag{5}$$

Equations (1-4) govern the motion of a structure subjected to supersonic aerodynamic forces.

III. Finite Element Discretization

We apply the finite element method to discretize the governing equations for the stiffened plates and shells in the supersonic flow. The plate or shell is modeled with the three-dimensional degenerated shell element and the stiffener with the three-dimensional degenerated curved beam element. The curved beam element uses the same nodes as the shell element by introducing the offsets between the neutral axis of stiffener and the middle surface of shell. Hence a panel with stiffeners will not increase the number of nodes as compared to one without stiffeners. The compatibility between stiffener and plate/shell is achieved and the completeness requirement is satisfied. These shell and curved beam elements have been employed in the geometrically nonlinear bending analysis of stiffened laminated composite plates and shells by Liao and Reddy,[20] and good results were obtained. We will not go through the details of these two elements and only describe them very briefly in the following.

A. Three-Dimensional Degenerated Shell Element

Figure 1 shows the geometry of a three-dimensional degenerated shell element that is degenerated from the three-dimensional solid isoparametric element by imposing two constraints.[20] The coordinates of a typical point in the element can be interpolated by

$$x_i = \sum_{k=1}^{n} \phi_k(\xi,\eta)\left(x_i^k + \frac{\zeta}{2} h_k\, {}^t e_{3i}^k\right) \qquad (i = 1, 2, 3) \tag{6}$$

and the displacements by

$$u_i = \sum_{k=1}^{n} \phi_k(\xi,\eta)\left[u_i^k + \frac{\zeta}{2} h_k(\theta_1^k\, {}^t e_{1i}^k - \theta_2^k\, {}^t e_{2i}^k)\right] \quad (i = 1, 2, 3) \tag{7}$$

In Eqs. (6) and (7), ξ, η, and ζ are the natural coordinates that lie between -1 and 1, n is the number of nodes of an element, $\phi_k(\xi, \eta)$ is the Lagrange family of interpolation functions of a two-dimensional element, the right-hand superscript k means the kth node, h_k is the thickness at node k, and ${}^t e_{3i}^k$ are the components of unit vector normal to the shell midsurface at node k. At each node there are five degrees of freedom, i.e., u_1^k, u_2^k, u_3^k, θ_1^k, and θ_2^k. From Eqs. (6) and (7), we can formulate the displacement interpolation matrix $[N_s]$ and the relation matrix between linear strains and nodal displacements $[B_s]$. Using Eqs. (1-4), the finite element equation of motion for the three-dimensional degenerated shell element in supersonic flow is

$$[M_s^e]\{\ddot{\Delta}_s^e\} + [D_s^e]\{\dot{\Delta}_s^e\} + ([A_s^e] + [K_s^e])\{\Delta_s^e\} = \{0\} \tag{8}$$

where $[M_s^e]$, $[D_s^e]$, $[A_s^e]$ and $[K_s^e]$ are the mass, aerodynamic damping, aerodynamic, and linear stiffness matrices, respectively, for the shell element; and $\{\ddot{\Delta}_s^e\}$, $\{\dot{\Delta}_s^e\}$, and $\{\Delta_s^e\}$ are the nodal acceleration, velocity, and displacement vectors, respectively, for the shell element. The matrices are defined as

$$\begin{aligned}
[M_s^e] &= \int_{V_e} \rho [N_s]^T [N_s]\, dV_e \\
[D_s^e] &= \int_{V_e} g [N_s^3]^T [N_s^3]\, dV_e \\
[A_s^e] &= \int_{V_e} \lambda \frac{\partial [N_s^3]^T}{\partial x_1} [N_s^3]\, dV_e \\
[K_s^e] &= \sum_{q=1}^{\text{nol}} \int_{V_e^{(q)}} [B_s]^T [C]^{(q)} [B_s]\, dV_e^{(q)}
\end{aligned} \tag{9}$$

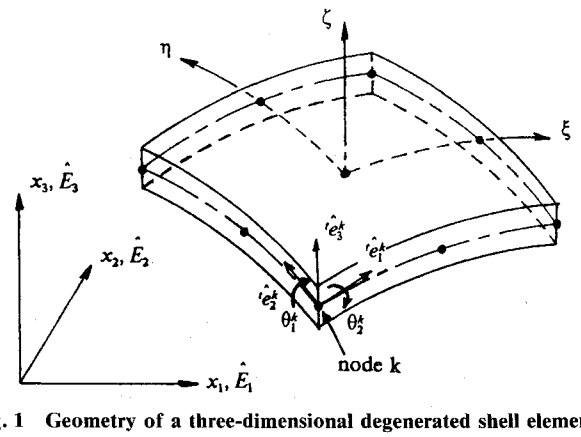

Fig. 1 Geometry of a three-dimensional degenerated shell element.

where the superscript T denotes the transpose of a matrix, $[N_s^3]$ is the displacement interpolation matrix for the displacement u_3 only, nol means the number of layers of a laminate, $[C]^{(q)}$ is the constitutive matrix of the qth layer, and V_e is the volume of each element. Since we neglect the transverse normal stress and strain for the plate and shell structures, $[C]^{(q)}$ is of order 5×5 and can be found in Ref. 20. In general, $[C]^{(q)}$ is given in the plate/shell rectangular Cartesian coordinate system. If we consider the skew plate and use the oblique Cartesian coordinate system, $[C]^{(q)}$ should be transformed to the oblique coordinate system by the following equation[18]:

$$[C']^{(q)} = [T][C]^{(q)}[T]^T \tag{10}$$

where

$$[T] = \begin{bmatrix} 1 & \tan^2\theta & 0 & 0 & -2\tan\theta \\ 0 & 1/\cos^2\theta & 0 & 0 & 0 \\ 0 & 0 & 1/\cos\theta & 0 & 0 \\ 0 & 0 & -\tan\theta & 1 & 0 \\ 0 & -\tan\theta/\cos\theta & 0 & 0 & 1/\cos\theta \end{bmatrix}$$

and where θ is the skew angle (see Fig. 2); $[C']^{(q)}$ is the constitutive matrix relating the contravariant components of the Cauchy stress tensor and the covariant components of the infinitesimal strain tensor.[18]

B. Three-Dimensional Degenerated Curved Beam Element

Figure 3 shows the geometry of a three-dimensional degenerated curved beam element with rectangular cross section that is also degenerated from the three-dimensional solid isoparametric element by imposing two constraints.[20] The coordinates of a typical point in the element can be interpolated by

$$x_i = \sum_{k=1}^{n} \phi_k(\xi)\left[x_i^k + \left(\frac{\zeta}{2}a_k + \Delta_k^\zeta\right){}^t e_{3i}^k + \left[\frac{\eta}{2}b_k + \Delta_k^\eta\right]{}^t e_{2i}^k\right]$$

$$(i = 1, 2, 3) \tag{11}$$

where Δ_k^ζ and Δ_k^η are the offsets in the directions ${}^t\hat{e}_3^k$ and ${}^t\hat{e}_2^k$, respectively, at node k, $\phi_k(\xi)$ is the Lagrange family of interpolation functions of a line element, and x_i^k are the Cartesian coordinates at node k. From Eq. (11), the displacement components can be written as

$$u_i = \sum_{k=1}^{n} \phi_k(\xi)\left\{u_i^k + \left[\left(\frac{\eta}{2}b_k + \Delta_k^\eta\right){}^t e_{3i}^k - \left(\frac{\zeta}{2}a_k + \Delta_k^\zeta\right){}^t e_{1i}^k\right]\theta_2^k + \left(\frac{\zeta}{2}a_k + \Delta_k^\zeta\right){}^t e_{1i}^k\,\theta_1^k - \left(\frac{\eta}{2}b_k + \Delta_k^\eta\right){}^t e_{1i}^k\,\theta_3^k\right\}$$

$$(i = 1, 2, 3) \tag{12}$$

At each node there are six degrees of freedom, i.e., u_1^k, u_2^k, u_3^k, θ_1^k, θ_2^k, and θ_3^k. From Eqs. (11) and (12), we can formulate the displacement interpolation matrix $[N_b]$ and the relation matrix between linear strains and nodal displacements $[B_b]$. From Hamilton's principle without the aerodynamic force term, the finite element equation of motion for the beam element is given by

$$[M_b^e]\{\ddot{\Delta}_b^e\} + [K_b^e]\{\Delta_b^e\} = \{0\} \tag{13}$$

where $\{\ddot{\Delta}_b^e\}$ and $\{\Delta_b^e\}$ are the element nodal acceleration and displacement vectors, and $[M_b^e]$ and $[K_b^e]$ are the element mass and stiffness matrices, which are defined as

$$[M_b^e] = \int_{V_e} \rho[N_b]^T[N_b]\,dV_e$$
$$[K_b^e] = \sum_{q=1}^{\text{nol}} \int_{V_e^{(q)}} [B_b]^T[C]^{(q)}[B_b]\,dV_e^{(q)} \tag{14}$$

where the constitutive matrix $[C]^{(q)}$ for each layer of the laminated composite beam is chosen the same as that for the laminated composite plate/shell.

C. Shell Element with Stiffeners

If the shell element is stiffened with stiffeners, then the finite element equations of motion of the stiffened shell ele-

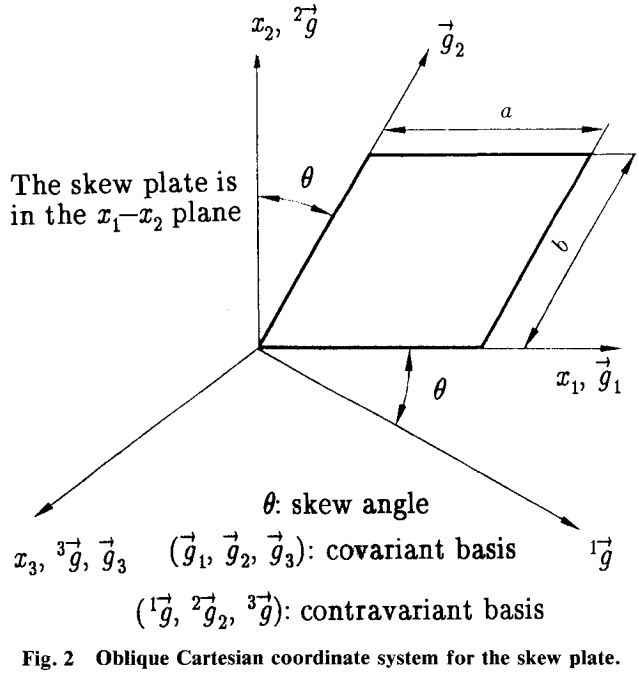

Fig. 2 Oblique Cartesian coordinate system for the skew plate.

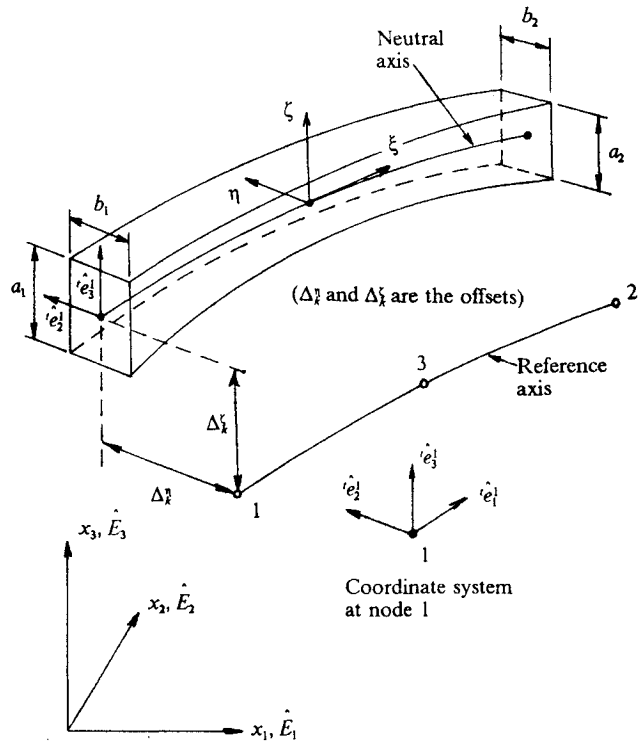

Fig. 3 Geometry of a three-dimensional degenerated curved beam element.

ment in the supersonic flow are obtained by combining Eqs. (8) and (13), which are

$$([M_s^e] + [M_b^e])\{\ddot{\Delta}^e\} + [D_s^e]\{\dot{\Delta}^e\} + ([A_s^e] + [K_s^e] + [K_b^e])\{\Delta^e\} = \{0\} \tag{15}$$

where $\{\ddot{\Delta}^e\}$, $\{\dot{\Delta}^e\}$, and $\{\Delta^e\}$ are the nodal acceleration, velocity, and displacement vectors, respectively, and have six degrees of freedom at each node as the beam element. In the present study, two kinds of stiffener orientations with respect to the plate/shell coordinate axes are used.[20,21]

D. Characteristic Equations of the Stiffened Plate/Shell

Assembling the finite element equations of motion for each element, we obtain the finite element equations of motion for the whole stiffened plate or shell as follows:

$$[M]\{\ddot{\Delta}\} + [D]\{\dot{\Delta}\} + ([A] + [K])\{\Delta\} = \{0\} \tag{16}$$

where $[M]$, $[D]$, $[A]$, and $[K]$ are the mass, aerodynamic damping, aerodynamic, and stiffness matrices for the system, respectively, and are all of order $m \times m$. Since the mass matrix in Eq. (16) includes the rotary inertia, $[M]$ and $[D]$ are not proportional [this can be easily seen from the definitions of $[M_s^e]$ and $[D_s^e]$ in Eq. (9)]. Therefore, Eq. (16), as written in the configuration space, does not lend itself to standard eigenvalue solution algorithms. Thus, the approach that transforms the problem from the configuration space to a state space is adopted here. By making the transformation to the state space, Eq. (16) becomes

$$\begin{Bmatrix} [M] & [0] \\ [0] & [I] \end{Bmatrix} \begin{pmatrix} \{\ddot{\Delta}\} \\ \{\dot{\Delta}\} \end{pmatrix} + \begin{Bmatrix} [D] & [A] + [K] \\ -[I] & [0] \end{Bmatrix} \begin{pmatrix} \{\dot{\Delta}\} \\ \{\Delta\} \end{pmatrix} = \begin{pmatrix} \{0\} \\ \{0\} \end{pmatrix} \tag{17}$$

where $[I]$ is the unit matrix. Equation (17) also can be expressed as

$$[M^*]\{\dot{y}(t)\} + [K^*]\{y(t)\} = \{0\} \tag{18}$$

The solution to Eq. (18) is assumed in the form of $\{y(t)\} = \{\varphi\}e^{\Omega t}$. Substituting the assumed solution into Eq. (18), we get

$$\Omega[M^*]\{\varphi\} + [K^*]\{\varphi\} = \{0\} \tag{19}$$

Since $[M^*]$ is symmetric and $[K^*]$ is unsymmetric, the characteristic values of Eq. (19) are complex in general. Hence Ω can be expressed as $\Omega_r = \bar{\alpha}_r \pm i\omega_r$ $(r = 1, 2, \ldots, m)$. Correspondingly, the eigenvectors also occur in pairs of complex conjugates, $\{\varphi\}_r = \{A\}_r \pm \{B\}_r$ $(r = 1, 2, \ldots, m)$. The solution $\{y(t)\}$ of Eq. (18) can now be written as

$$\{y(t)\} = e^{(\bar{\alpha}+i\omega)t}(\{A\} + i\{B\}) = e^{\bar{\alpha}t}e^{i\omega t}\begin{bmatrix} (a_1^2 + b_1^2)^{0.5}e^{i\phi_1} \\ (a_2^2 + b_2^2)^{0.5}e^{i\phi_2} \\ \vdots \\ (a_{2m}^2 + b_{2m}^2)^{0.5}e^{i\phi_{2m}} \end{bmatrix} = e^{\bar{\alpha}t}\begin{bmatrix} r_1\, e^{i(\omega t+\phi_1)} \\ r_2\, e^{i(\omega t+\phi_2)} \\ \vdots \\ r_{2m}\, e^{i(\omega t+\phi_{2m})} \end{bmatrix} \tag{20}$$

where ω is the frequency of vibration and

$$\{A\} = \begin{bmatrix} a_1 \\ a_2 \\ \vdots \\ a_{2m} \end{bmatrix}, \quad \{B\} = \begin{bmatrix} b_1 \\ b_2 \\ \vdots \\ b_{2m} \end{bmatrix}, \quad \phi_k = \tan^{-1}\left(\frac{b_k}{a_k}\right)$$

$$(0 \le \phi_k \le \pi)$$

$$r_k = (a_k^2 + b_k^2)^{0.5}$$

The real part of $\{y(t)\}$ is

$$Re\{y(t)\} = e^{\bar{\alpha}t}\begin{bmatrix} r_1\cos(\omega t + \phi_1) \\ r_2\cos(\omega t + \phi_2) \\ \vdots \\ r_{2m}\cos(\omega t + \phi_{2m}) \end{bmatrix} \tag{21}$$

From Eq. (21), we can see that if $\bar{\alpha}$ is negative, any disturbance to the stiffened plate or shell in the supersonic flow decays with time, that is, the system is stable. On the contrary, if $\bar{\alpha}$ is positive, then the amplitude of vibration grows exponentially with time, that is, the system is unstable or fluttering. Hence by solving Eq. (18) for the characteristic values, we can study the stability of the structure and also find the critical dynamic pressure and the associated flutter mode. The behavior of a stiffened plate or shell is demonstrated by plotting the variation of $(\bar{\alpha} + i\omega)$ with increasing dynamic pressure λ in the following section of numerical results.

IV. Numerical Results and Discussion

In this section we use the preceding finite element model to investigate the effects of various parameters, such as skew angles, lamination schemes, subtended angle, and number and position of stiffeners, on the flutter instability of stiffened plates and shells. After the convergence study, we found that the 3×3 uniform mesh (including nine-node shell elements and three-node beam elements) is sufficient to provide accurate flutter results. Hence in the following analyses this mesh is used to model the stiffened plate or shell whose four sides have the same length. Three kinds of boundary conditions are considered: C-F-F-F, S-S-S-S, and C-C-C-C (C: clamped, F: free, S: simply supported). For the C-F-F-F plate, the direction of airflow is parallel to the clamped edge. For the other boundary conditions, the airflow is in the x_1 direction. In the following numerical examples, we include the aerodynamic damping by assuming $\mu/M = 0.01$, and hence the aerodynamic damping matrix in Eq. (16) is included. First, we will present some results of nonstiffened plates which are compared with those available in the literature to demonstrate the accuracy of the present finite element model. Then we will study the flutter instability of stiffened isotropic and laminated composite plates and shells. Nondimensionalized quantities are used to present the results.

For isotropic material, the nondimensionalized frequency is defined as $\bar{\omega} = \omega a^2(\rho h/D)^{(0.5)}$, where $D = Eh^3/[12(1 - \nu^2)]$, E is Young's modulus, h is the thickness of the plate/shell, and ν is Poisson's ratio. The nondimensionalized dynamic pressure is defined as $\bar{\lambda} = \lambda(a^3/D)$.

For laminated composite material, $\bar{\omega} = (\omega a^2/h)(\rho/E_2)^{(0.5)}$, where E_2 is Young's modulus normal to the fiber direction of the orthotropic material, and h is the thickness of the laminate. Also, $\bar{\lambda} = \lambda(a^3/E_2h^3)$. The following material properties will be used for the laminated composite material: $\nu_{12} = 0.28$, $E_1 = 3.1 \times 10^7$ psi, $E_2 = 2.7 \times 10^6$ psi, and $G_{12} = G_{13} = G_{23} = 0.75 \times 10^6$ psi, Additional results can be found in Ref. 21.

A. Effect of Skew Angle on the Flutter Bounds of Isotropic Square Plates

Table 1 gives the first six in-vacuo natural frequencies $\bar{\omega}_i$, critical dynamic pressures $\bar{\lambda}_{cr}$, and the corresponding critical frequencies $\bar{\omega}_{cr}$ for the C-F-F-F, S-S-S-S, and C-C-C-C isotropic plates, respectively. The plate properties are $a/h = 40$ and $\nu = 0.3$. From Table 1, we see that the boundary condition significantly influences $\bar{\lambda}_{cr}$, and $\bar{\lambda}_{cr}$ decreases as the skew angle increases for the C-F-F-F boundary condition, whereas $\bar{\lambda}_{cr}$ increases as the skew angle increases for the S-S-S-S and C-C-C-C boundary conditions. For each case in

Table 1 In-vacuo natural frequencies $\bar{\omega}_i$, $\bar{\lambda}_{cr}$, and $\bar{\omega}_{cr}$ for C-F-F-F, S-S-S-S, and C-C-C-C isotropic plates

	C-F-F-F, θ, deg			S-S-S-S, θ, deg			C-C-C-C, θ, deg		
	0	15	30	0	15	30	0	15	30
$\bar{\omega}_{cr}$	6.430[a]	—	—	42.972[b]	—	—	65.53[b]	—	—
	6.441	7.53	8.697	42.101	43.358	48.27	65.26	67.91	79.02
$\bar{\lambda}_{cr}$	58.35[a]	—	—	512.33[b]	—	—	852.73[b]	—	—
	57.85	46.275	40.411	498.01	521.47	614.89	867.66	925.00	1212.3
$\bar{\omega}_1$	3.468	3.580	3.929	19.736	20.918	25.335	36.073	38.290	46.312
$\bar{\omega}_2$	8.473	8.664	9.381	50.354	49.267	54.087	78.259	78.069	88.582
$\bar{\omega}_3$	21.385	22.335	25.427	50.354	57.509	74.818	78.259	88.359	113.79
$\bar{\omega}_4$	27.200	26.374	26.049	80.559	81.944	89.56	115.69	120.12	137.83
$\bar{\omega}_5$	31.067	34.020	41.738	106.31	112.78	136.21	158.68	169.18	207.31
$\bar{\omega}_6$	53.817	52.351	51.604	106.31	116.73	138.44	159.53	173.22	211.24

[a]Reference 22. [b]Reference 15.

Table 2 In-vacuo natural frequencies $\bar{\omega}_i$, $\bar{\lambda}_{cr}$, and $\bar{\omega}_{cr}$ for C-C-C-C cross-ply [0/90] plates

	$\bar{\omega}_1$	$\bar{\omega}_2$	$\bar{\omega}_3$	$\bar{\omega}_4$	$\bar{\omega}_5$	$\bar{\omega}_6$	$\bar{\omega}_{cr}$	λ_{cr}
Present	15.296	31.411	31.411	42.474	57.78	58.026	26.734	142.1
IE[17]	16.22	33.82	33.82	46.35	63.84	65.39	28.99	163.23
Series[17]	16.71	33.71	33.71	46.14	62.22	62.36	29.79	173.31

Table 3 Effect of number of layers on $\bar{\lambda}_{cr}$ and $\bar{\omega}_{cr}$ for C-C-C-C cross-ply [0/90/. . .] and angle-ply [45/ − 45/. . .] plates

No. of layers	Cross ply [0/90/. . .]		Angle ply [45/ − 45/. . .]	
	$\bar{\omega}_{cr}$	$\bar{\lambda}_{cr}$	$\bar{\omega}_{cr}$	$\bar{\lambda}_{cr}$
2	26.734	142.095	26.155	139.259
4	33.565	218.311	32.808	214.015
6	34.516	229.956	33.806	226.667
8	34.827	233.778	34.149	231.110
10	34.975	235.644	34.297	233.007
12	35.040	236.652	34.425	234.074

Table 1, the frequencies of the first and second modes, $\bar{\omega}_1$ and $\bar{\omega}_2$, approach each other and coalesce as $\bar{\lambda}$ is increased from zero. Before $\bar{\omega}_1$ and $\bar{\omega}_2$ coalesce, the corresponding $\bar{\alpha}_1$ and $\bar{\alpha}_2$ are equal and negative, and so the system is stable. After $\bar{\omega}_1$ and $\bar{\omega}_2$ meet and $\bar{\lambda}$ is increased continuously, $\bar{\omega}_1$ and $\bar{\omega}_2$ remain the same, but $\bar{\alpha}_1$ and $\bar{\alpha}_2$ will deviate from each other where $\bar{\alpha}_1$ becomes more negative, whereas $\bar{\alpha}_2$ becomes positive. When $\bar{\alpha}_2$ becomes positive, the corresponding $\bar{\lambda}$ value is the $\bar{\lambda}_{cr}$, and the system becomes unstable (i.e., flutter begins). The flutter mode is formed by the first and second natural vibration modes for all cases in Table 1.

B. Effect of the Number of Layers on the Flutter Bounds of C-C-C-C Cross-Ply [0/90/. . .] and Angle-Ply [45/ − 45/. . .] Square Plates

The antisymmetric cross-ply and angle-ply plates have the following properties: skew angle $\theta = 0$ deg and $a/h = 20$. Table 2 gives the first six in-vacuo natural frequencies $\bar{\omega}_i$, critical dynamic pressures $\bar{\lambda}_{cr}$, and the corresponding critical frequencies $\bar{\omega}_{cr}$ for the C-C-C-C [0/90] plate. The present results are compared with those in Ref. 17 [which used an integral equation (IE) method and a series solution method], and we see that the present values are all lower than those of Ref. 17. The reason is that Ref. 17 was based on the classical lamination theory, which neglects the transverse shear deformations, whereas the present study includes them. Table 3 shows the effect of number of layers on $\bar{\lambda}_{cr}$ and $\bar{\omega}_{cr}$ for the C-C-C-C cross-ply [0/90/. . .] and angle-ply [45/ − 45/. . .] plates (the thickness of the laminate is fixed, whereas the number of layers is changed). For each case in Table 3, the flutter mode associated with $\bar{\lambda}_{cr}$ is formed by the first and second natural vibration modes. From Table 3, we see that $\bar{\lambda}_{cr}$ approaches a constant value as the number of layers increases. The reason is that the bending-extension coupling stiffnesses of an antisymmetric laminate become very small when the number of layers increases.[23]

C. Effects of Position and Number of Stiffeners on the Flutter Bounds of C-C-C-C Isotropic Square Plates

Figure 4 shows some geometric configurations of stiffened square plates considered, in which $a/h = 40$, $f/h = 1.5$, and $e/a = 0.01$. The air flows over the upper surface of the plate in the x_1 direction. The stiffeners are located on the lower surface of the plate. Figure 5 shows the characteristic curves of $(\bar{\alpha} + i\bar{\omega})$ vs $\bar{\lambda}$ for the C-C-C-C stiffened plates shown in Figs. 4a and 4b. From Fig. 5, we see that the first flutter mode for the stiffened plate in Fig. 4a is formed by the first and third vibration modes, whereas that for the stiffened plate in Fig. 4b is formed by the first and second modes. The difference is because the flutter mode is formed by those two modes that are symmetric to the airflow direction (i.e., x_1 direction). Table 4 gives values of $\bar{\lambda}_{cr}$ and $\bar{\omega}_{cr}$ for those stiffened plates in Fig. 4. From Table 4, we see that the stiffener must be located in the airflow direction to increase $\bar{\lambda}_{cr}$. If the stiffener is perpendicular to the airflow direction, $\bar{\lambda}_{cr}$ is even lower than that without a stiffener. Also, $\bar{\lambda}_{cr}$ for the stiffened plate in Fig. 4c is lower than that for Fig. 4a, even though the former has one extra stiffener normal to the airflow. The physical explanation of this phenomenon is that the natural frequencies of adjacent modes that form the first flutter mode become closer together when the extra stiffener is added. Comparing values of $\bar{\lambda}_{cr}$ for stiffened plates in Figs. 4a, 4f, and 4g, we see that the stiffening effect is best if we put one stiffener in the center instead of using several whose total width equals that of the single stiffener (all are in the airflow direction). Finally, from Table 4, we see that $\bar{\lambda}_{cr}$ is increased if we increase the number of stiffeners with the same size, but $\bar{\lambda}_{cr}$ for the plate with two equally spaced stiffeners normal to the airflow is still lower than that without any stiffener.

D. Effect of Skew Angle θ on the Flutter Bounds of C-C-C-C Stiffened Isotropic Square Plates

We consider the stiffened plates shown in Figs. 4a and 4b, except that their shapes are changed from square to parallelogram. For the stiffened skew plates considered here, $a/h = 40$, $f/h = 1.5$, and $e/a = 0.01$. The airflow is in the x_1 direction. Figure 6 shows the effect of skew angle on the characteristic curves of $(\bar{\alpha} + i\bar{\omega})$ vs $\bar{\lambda}$ for the C-C-C-C stiffened plate shown in Fig. 4a. From Fig. 6, we see that the first flutter mode is formed by the first and second natural vibration modes for $\theta \neq 0$ deg, instead of the first and third modes (whose mode shapes are symmetric with respect to the airflow direction) for $\theta = 0$. This is because the mode shapes are no longer symmetric with respect to the airflow direction when $\theta \neq 0$. Therefore, the flutter mode is formed by the neighboring modes. Table 5

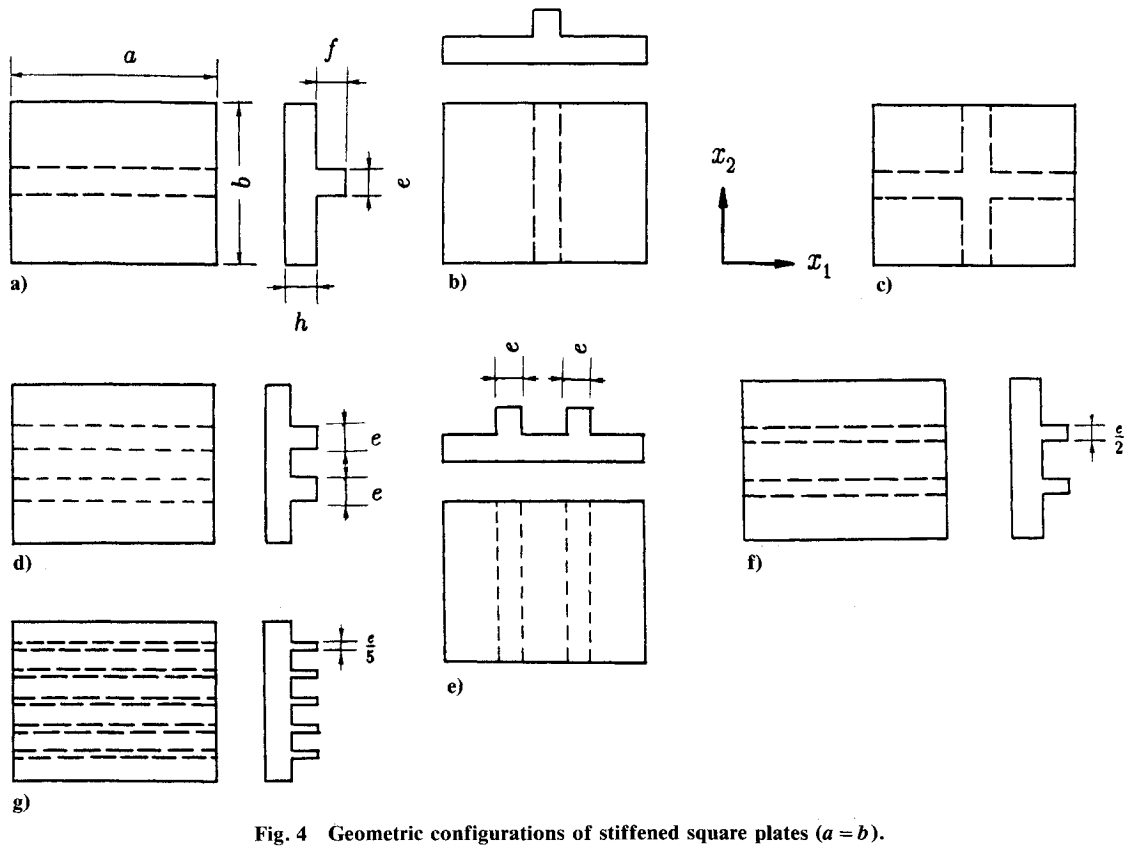

Fig. 4 Geometric configurations of stiffened square plates ($a = b$).

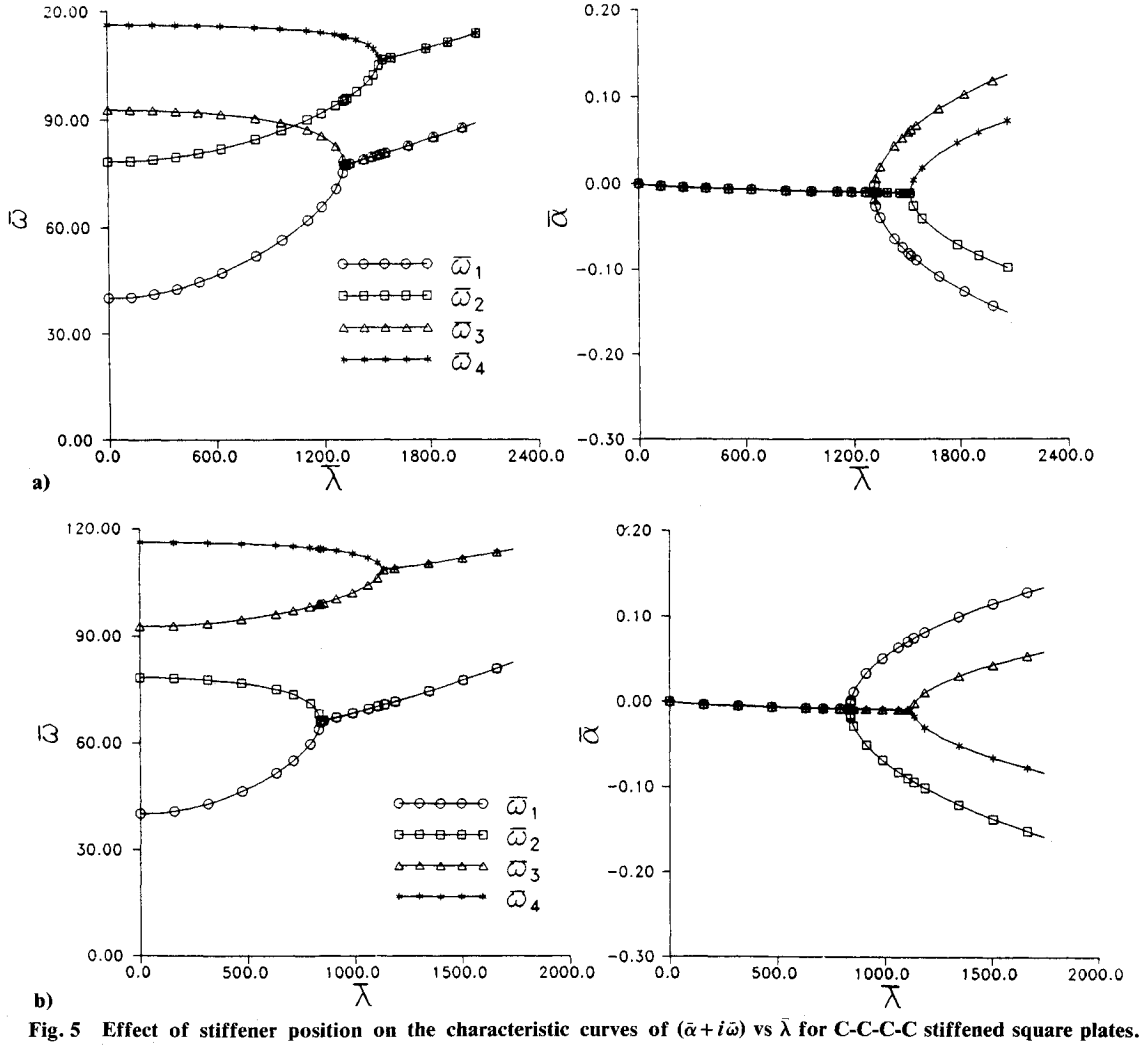

Fig. 5 Effect of stiffener position on the characteristic curves of ($\bar{\alpha} + i\bar{\omega}$) vs $\bar{\lambda}$ for C-C-C-C stiffened square plates.

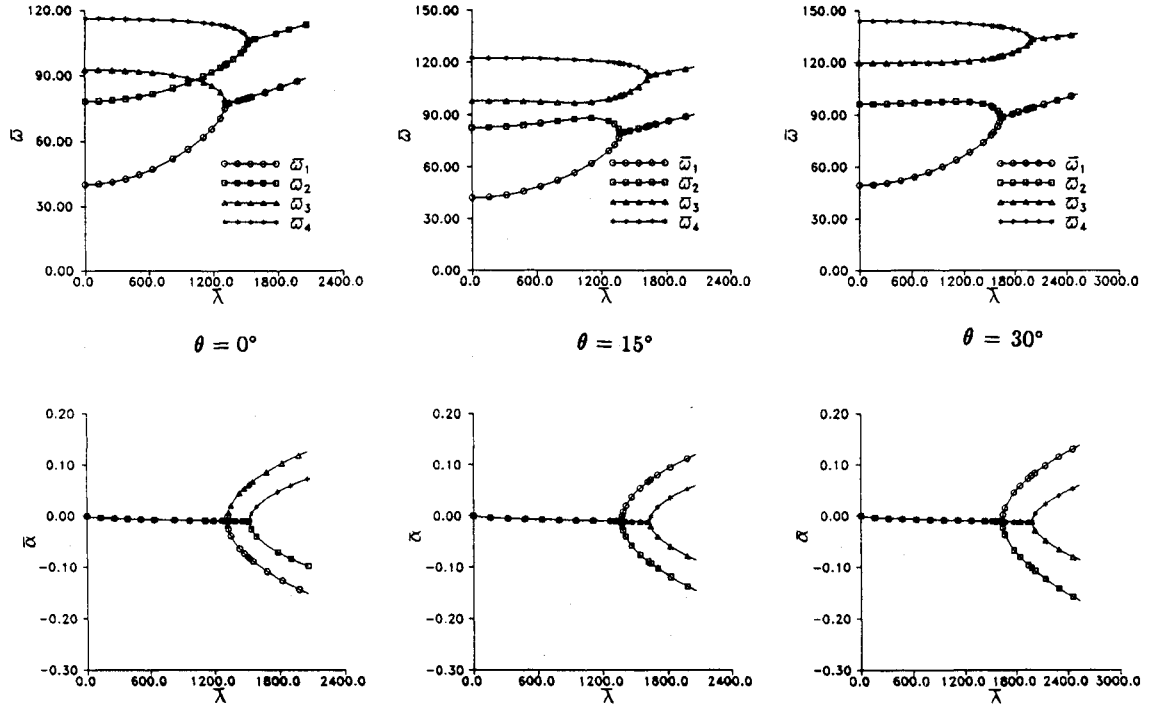

Fig. 6 Effect of skew angle on the characteristic curves of $(\bar{\alpha}+i\bar{\omega})$ vs $\bar{\lambda}$ for C-C-C-C stiffened square isotropic plate (in Fig. 4a).

Table 4 Values of $\bar{\lambda}_{cr}$ and $\bar{\omega}_{cr}$ for C-C-C-C stiffened isotropic plates in Fig. 4

Figure	$\bar{\omega}_{cr}$	$\bar{\lambda}_{cr}$
4a	77.234	1315.322
4b	65.872	840.716
4c	77.479	1294.750
4d	79.663	1434.209
4e	67.358	859.470
4f	73.543	1172.723
4g	72.262	1121.219

Table 5 Effect of skew angle on $\bar{\lambda}_{cr}$ and $\bar{\omega}_{cr}$ for C-C-C-C stiffened isotropic plates

	Stiffened plate in Fig. 4a		Stiffened plate in Fig. 4b	
θ, deg	$\bar{\omega}_{cr}$	$\bar{\lambda}_{cr}$	$\bar{\omega}_{cr}$	$\bar{\lambda}_{cr}$
0	77.234	1315.322	65.872	840.716
15	79.428	1375.428	69.895	941.428
30	88.312	1632.384	83.407	1307.508

Table 6 Values of $\bar{\lambda}_{cr}$ and $\bar{\omega}_{cr}$ for C-C-C-C stiffened isotropic cylindrical shells in Fig. 7

Figure	$\bar{\omega}_{cr}$	$\bar{\lambda}_{cr}$
7a	81.001	1343.164
7b	70.103	854.266
7c	81.210	1322.484
Without stiffener	69.439	879.620

shows the effect of skew angle on $\bar{\lambda}_{cr}$ and $\bar{\omega}_{cr}$ for the stiffened plates in Figs. 4a and 4b. For both cases, $\bar{\lambda}_{cr}$ and $\bar{\omega}_{cr}$ increase as θ increases.

E. Effects of Position and Number of Stiffeners on the Flutter Bounds of C-C-C-C Isotropic Cylindrical Shells

Figure 7 shows three geometric configurations of stiffened cylindrical shells that have the following properties: $a = b$, $a/h = 40$, $f/h = 1.5$, and $e/a = 0.01$, and subtended angle $b/r = 0.2$ (r is the shell radius). The air flows over the upper

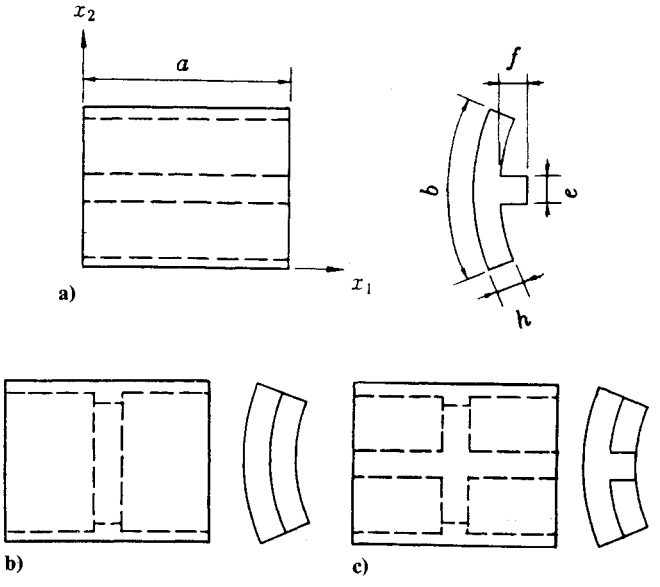

Fig. 7 Geometric configurations of stiffened cylindrical shells.

surface of the shell in the x_1 direction. The stiffeners are located on the lower surface of the shell. Table 6 gives values of $\bar{\lambda}_{cr}$ and $\bar{\omega}_{cr}$ for these stiffened cylindrical shells in Fig. 7. From Table 6, we see that the stiffener must be located in the airflow direction for the maximum $\bar{\lambda}_{cr}$ for these shells. If the stiffener is perpendicular to the airflow direction, $\bar{\lambda}_{cr}$ is even lower than that without any stiffener. Also $\bar{\lambda}_{cr}$ for the stiffened shell in Fig. 7c is lower than that in Fig. 7a, even though the former has an extra stiffener normal to the airflow and the latter does not. The physical explanation is similar to that for the stiffened plates in Figs. 4a and 4c.

F. Effects of Position and Number of Stiffeners on the Flutter Bounds of C-C-C-C Angle-Ply (45/−45/45/−45) Plates

The stiffened angle-ply laminates considered here have the configurations shown in Figs. 4a–4c. The geometries of angle-ply (45/−45/45/−45) laminates are: $a = b$, $a/h = 20$, $f/h = 1.5$, and $e/a = 0.01$. The stiffeners also have four layers and

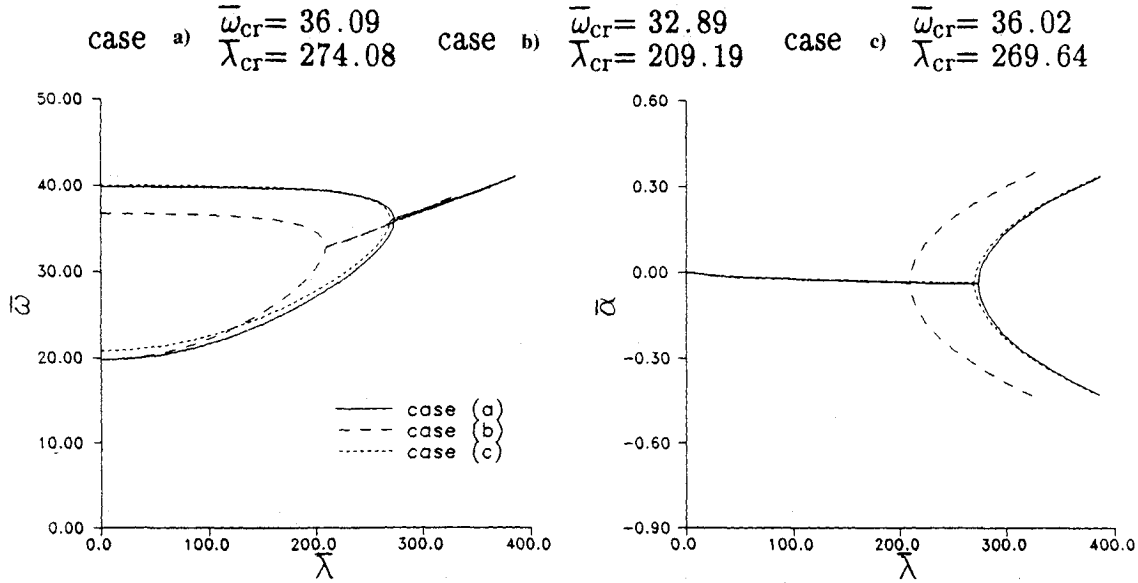

Fig. 8 Effects of stiffener position and number on the characteristic curves of $(\bar{\alpha}+i\bar{\omega})$ vs $\bar{\lambda}$ for C-C-C-C angle-ply [45/−45/45/−45] plates.

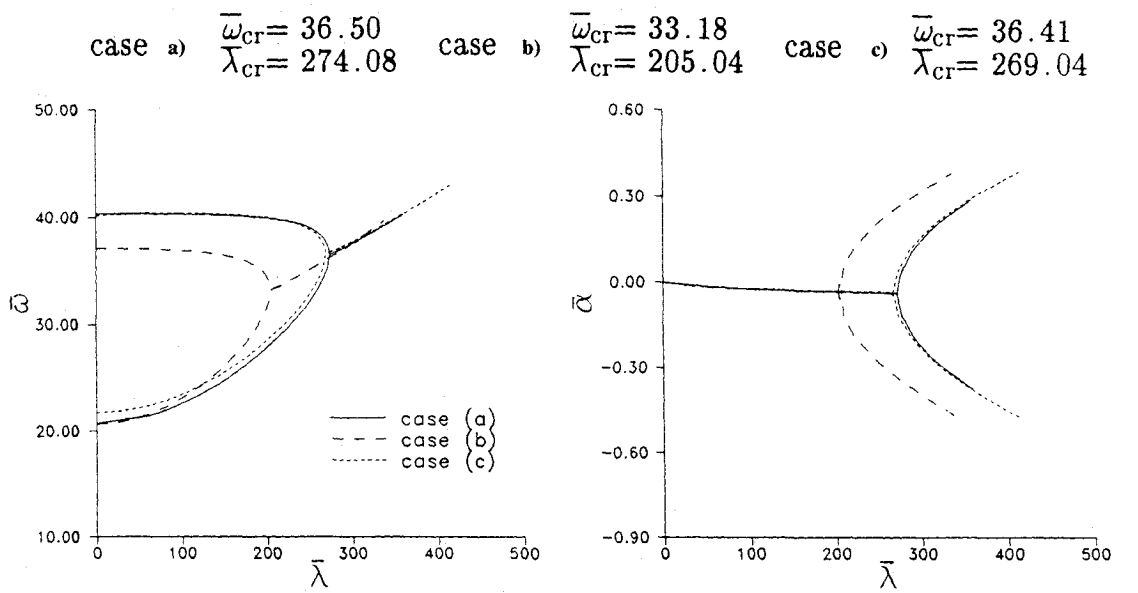

Fig. 9 Effects of stiffener position and number on the characteristic curves of $(\bar{\alpha}+i\bar{\omega})$ vs $\bar{\lambda}$ for C-C-C-C angle-ply [45/−45/45/−45] cylindrical shells.

the same lamination scheme as that of the shells. Figure 8 shows the characteristic curves of $(\bar{\alpha}+i\bar{\omega})$ vs $\bar{\lambda}$ and the values of $\bar{\lambda}_{cr}$ and $\bar{\omega}_{cr}$ for the C-C-C-C stiffened angle-ply (45/−45/45/−45) plates. From Fig. 8, we see that the stiffener must be located in the airflow direction for the maximum $\bar{\lambda}_{cr}$ for these configurations. If the stiffener is perpendicular to the airflow, $\bar{\lambda}_{cr}$ is even lower than that without any stiffener. Also, $\bar{\lambda}_{cr}$ for the stiffened angle-ply laminate in Fig. 4c is lower than that in Fig. 4a, even though the former has a stiffener normal to the airflow and the latter does not.

G. Effect of Subtended Angle on the Flutter Bounds of C-C-C-C Laminated Cylindrical Shells

The properties of laminated cylindrical shells $(\alpha/-\alpha/\alpha/-\alpha)$ considered are: $a=b$ and $a/h=20$. Table 7 shows the effect of subtended angle on $\bar{\lambda}_{cr}$ and $\bar{\omega}_{cr}$ for C-C-C-C angle-ply $(\alpha/-\alpha/\alpha/-\alpha)$ cylindrical shells, in which $\alpha=0$, 30, 45, 60, and 90 deg, respectively. For some lamination schemes ($\alpha=0$, 30, and 90 deg), $\bar{\lambda}_{cr}$ increases as the subtended angle increases (i.e., fix b and decrease r). But for some lamination schemes ($\alpha=45$ and 60 deg), $\bar{\lambda}_{cr}$ decreases as the subtended angle increases.

H. Effects of Position and Number of Stiffeners on the Flutter Bounds of C-C-C-C Angle-Ply (45/−45/45/−45) Cylindrical Shells

The stiffened C-C-C-C (45/−45/45/−45) cylindrical shells have the configurations as shown in Figs. 7a–7c, in which $a=b$, $a/h=20$, $f/h=1.5$, $e/a=0.01$, and subtended angle $b/r=0.2$. The stiffeners have four layers and the same lamination scheme. Figure 9 shows the characteristic curves of $(\bar{\alpha}+i\bar{\omega})$ vs $\bar{\lambda}$ and the values of $\bar{\lambda}_{cr}$ and $\bar{\omega}_{cr}$ for C-C-C-C stiffened angle-ply (45/−45/45/−45) cylindrical shells. From Fig. 9, we see that the stiffener must be located in the airflow direction for the largest $\bar{\lambda}_{cr}$. If the stiffener is perpendicular to the airflow, then $\bar{\lambda}_{cr}$ is even lower than that without any stiffener. Also, $\bar{\lambda}_{cr}$ for the stiffened shell in Fig. 7c is lower than that in Fig. 7a.

V. Conclusions

This study used the finite element method along with three-dimensional degenerated shell elements and three-dimensional degenerated curved beam elements to develop a finite element model to investigate the flutter instability of stiffened laminated composite plates and shells subjected to supersonic aerodynamic forces. The investigations were focused on the effects of skew angle, lamination scheme, subtended angle,

and number and position of stiffeners on the flutter instability of various plates and shells. The following conclusions can be drawn from the results.

1) For isotropic plates, the critical dynamic pressure $\bar{\lambda}_{cr}$ decreases as the skew angle increases for the C-F-F-F boundary condition, and $\bar{\lambda}_{cr}$ increases as the skew angle increases for the S-S-S-S and C-C-C-C boundary conditions.

2) For antisymmetric angle-ply plates $(45/-45/\ldots)$, $\bar{\lambda}_{cr}$ approaches a constant value as the number of layers increases.

3) The $\bar{\lambda}_{cr}$ is maximum when the stiffeners are oriented along the airflow direction.

4) For square plates, if the volume of the stiffeners is fixed, then putting the stiffeners close to the center of the plate along the airflow direction will obtain better stiffening effect.

5) For antisymmetric angle-ply $(\alpha/-\alpha/\alpha/-\alpha)$ cylindrical shells, the effect of subtended angle on $\bar{\lambda}_{cr}$ also depends on the lamination angle α.

References

[1]Dowell, E. H., "Panel Flutter: A Review of the Aeroelastic Stability of Plates and Shells," *AIAA Journal,* Vol. 8, No. 3, 1970, pp. 385–399.

[2]Olson, M. D., "Finite Elements Applied to Panel Flutter," *AIAA Journal,* Vol. 5, No. 12, 1967, pp. 2267–2270.

[3]Olson, M. D., "Some Flutter Solutions Using Finite Elements," *AIAA Journal,* Vol. 8, No. 4, 1970, pp. 747–752.

[4]Durvasula, S., "Flutter of Clamped Skew Panels in Supersonic Flow," *Journal of Aircraft,* Vol. 8, No. 4, 1971, pp. 461–466.

[5]Sander, G., Bon, C., and Geradin, M., "Finite Element Analysis of Supersonic Panel Flutter," *International Journal for Numerical Methods in Engineering,* Vol. 7, No. 3, 1973, pp. 379–394.

[6]Rossettos, J. N., and Tong, P., "Finite Element Analysis of Vibration and Flutter of Cantilever Anisotropic Plates," *Journal of Applied Mechanics,* Vol. 41, American Society of Mechanical Engineers, 1974, pp. 1075–1080; see also ASME Paper 74-WA/APM-15.

[7]Yang, T. Y., "Flutter of Flat Finite Element Panels in a Supersonic Potential Flow," *AIAA Journal,* Vol. 13, No. 11, 1975, pp. 1502–1507.

[8]Yang, T. Y., and Han, A. D., "Flutter of Thermally Buckled Finite Element Panels," *AIAA Journal,* Vol. 14, No. 7, 1976, pp. 975–977.

[9]Bismarck-Nasr, M. N., "Finite Element Method Applied to the Supersonic Flutter of Circular Cylindrical Shells," *International Journal for Numerical Methods in Engineering,* Vol. 10, No. 2, 1976, pp. 423–435.

[10]Yang, T. Y., and Sung, S. H., "Finite Element Panel Flutter in Three Dimensional Supersonic Unsteady Potential Flow," *AIAA Journal,* Vol. 15, No. 12, 1977, pp. 1677–1683.

[11]Hollowell, S. J., and Dugundji, J., "Aeroelastic Flutter and Divergence of Stiffness Coupled Graphite/Epoxy Cantilevered Plates," *Journal of Aircraft,* Vol. 21, No. 1, 1984, pp. 69–76.

[12]Lin, K. J., Lu, D. J., and Tarn, J. Q., "Flutter Analysis of Cantilevered Composite Plates in Subsonic Flow," *AIAA Journal,* Vol. 27, No. 8, 1989, pp. 1102–1109.

[13]Lin, Y. T., and Heller, R. A., "Some Flutter Solutions of Laminated Plates in Supersonic Flow," Virginia Polytechnic Inst. and State Univ., Research Rept., Dept. of Engineering Science and Mechanics, Blacksburg, VA, 1990.

[14]Mei, C., "A Finite Element Approach for Nonlinear Panel Flutter," *AIAA Journal,* Vol. 15, No. 8, 1977, pp. 1107–1110.

[15]Han, A. D., and Yang, T. Y., "Nonlinear Panel Flutter Using High-Order Triangular Finite Elements," *AIAA Journal,* Vol. 21, No. 10, 1983, pp. 1453–1461.

[16]Sarma, B. S., and Varadan, T. K., "Nonlinear Panel Flutter by Finite-Element Method," *AIAA Journal,* Vol. 26, No. 5, 1988, pp. 566–574.

[17]Srinivasan, R. S., and Babu, B. J. C., "Free Vibration and Flutter of Laminated Quadrilateral Plates," *Journal of Computers and Structures,* Vol. 27, No. 2, 1987, pp. 297–304.

[18]Lee, Z. Y., "Studies on the Elastic Stability of Laminated Composite Skew Plates Subjected to Biaxial Follower Forces," M.S. Thesis, Dept. of Mechanical Engineering, National Taiwan Inst. of Technology, Taipei, Taiwan, ROC, 1991.

[19]Bisplinghoff, R. L., and Ashley, H., *Principles of Aeroelasticity,* Wiley, New York, 1962.

[20]Liao, C. L., and Reddy, J. N., "Continuum-Based Stiffened Composite Shell Element for Geometrically Nonlinear Analysis," *AIAA Journal,* Vol. 27, No. 1, 1989, pp. 95–101.

[21]Sun, Y. W., "Elastic Stability of Stiffened Laminated Composite Plates and Shells in Supersonic Flow," M.S. Thesis, Dept. of Mechanical Engineering, National Taiwan Inst. of Technology, Taipei, Taiwan, ROC, 1992.

[22]Srinvinvasan, R. S., and Babu, B. J. C., "Flutter Analysis of Cantilevered Quadrilateral Plates," *Journal of Sound and Vibration,* Vol. 98, No. 1, 1985, pp. 45–53.

[23]Jones, R. M., *Mechanics of Composite Materials,* Scripta, Washington, DC, 1975.